The mechanism of H-bond rupture: the vibrational pre-dissociation of C_2H_2–HCl and C_2H_2–DCl

Marisian Pritchard,[a] Jessica Parr,[b] Guosheng Li,[b] Hanna Reisler[b] and Anthony J. McCaffery*[a]

Received 17th July 2007, Accepted 24th September 2007
First published as an Advance Article on the web 5th October 2007
DOI: 10.1039/b710967a

Pair correlated fragment rovibrational distributions are presented following vibrational predissociation of the C_2H_2–DCl van der Waals dimer initiated by excitation of the asymmetric (asym) C–H stretch. The only observed fragmentation pathways are DCl ($v = 0$; $j = 6$–9) + C_2H_2 ($\nu_2 = 1$; $j = 1$–5). These and previously reported data on the related C_2H_2–HCl species are analysed using the angular momentum (AM) method. Calculations accurately reproduce fragment rovibrational distributions following dissociation of the C_2H_2–HCl dimer initiated either by excitation of the asym C–H stretch or *via* the HCl stretch, and those from C_2H_2–DCl initiated *via* asym C–H stretch excitation. The calculations demonstrate that the dimer is bent at the moment of dissociation. Several geometries are found that lead to H-bond breakage *via* a clearly identified set of fragment quantum states. The results suggest a hierarchy in the disposal of excess energy and angular momentum between fragment vibration, rotation and recoil. Deposition of the largest portion of energy into a C_2H_2 vibrational state sets an upper limit on HCl rotation, which then determines the energy and AM remaining for C_2H_2 rotation and fragment recoil. Acceptor C_2H_2 vibrational modes follow a previously noted propensity, implying that the dissociating impulse must be able to induce appropriate nuclear motions both in the acceptor vibration *and* in rotation of the C_2H_2 fragment.

1. Introduction

The dissociation of vibrationally excited van der Waals (vdW) molecules continues to be a topic of great interest many years after vibrational predissociation (VP) in these weakly-bound complexes was first observed.[1] The spontaneous fragmentation of a species containing excess energy is important in a wide range of chemical and biological contexts. When this process involves the breaking of a hydrogen bond, it takes on an additional significance. VP is a low-energy event involving quantum levels located in a spectral region that is relatively uncluttered, thus initial states may be specified quite precisely and product states identified with a high degree of certainty. Key experimental observables in VP experiments are the dissociative lifetime and rovibrational distribution among the fragment species following dissociation.[2] Experiments in which fragment state rovibrational distributions are fully determined increase greatly our understanding of the mechanism of VP. Furthermore they contain clues as to the manner in which molecules deal with excess energy *e.g.* the role of intramolecular vibrational redistribution (IVR) prior to dissociation.

Highly excited small polyatomic molecules often exhibit signatures of non-statistical populations among their vibrational and rotational states, in marked contrast to molecules having high density of vibrational states. At some point as molecular complexity increases, excess energy, initially located within a specific mode, rapidly becomes delocalised as the molecule switches between iso-energetic configurations of its quantum states.[3] The extent of IVR becomes a significant issue in the VP of weakly bound complexes, which usually display nonstatistical VP, because of the disparity between the frequencies of the intermolecular modes of the complex and the intramolecular vibrational frequencies of the molecular subunits. In at least one theoretical treatment[4] the assumption that IVR precedes VP is an essential element. However, the molecular parameters that determine the extent of IVR in weakly bound complexes are not well characterised. High-resolution VP experiments have the capacity to characterise this change in molecular behaviour though the experimental difficulties mount rapidly as molecular complexity increases. In this context it is worth emphasising that vibrational resolution alone is rarely sufficient for this purpose since dynamical detail essential to full understanding of VP is contained also in the distribution of population among *rotational* states.

In this paper we present new, pair-correlated fragment rovibrational state distributions following the VP of C_2H_2–DCl, and a theoretical analysis of these as well as data on the closely related C_2H_2–HCl H-bonded complex recently reported by Li *et al.*[5] vdW molecules in which adducts are H-bonded to the π-electron system of acetylene have been known for some years.[6–10] The structures of complexes of C_2H_2 with HX and DX (X = halogen) have been studied using a number of spectroscopic techniques and their T-shaped

[a] *Department of Chemistry, University of Sussex, Brighton, UK BN19QJ*
[b] *Department of Chemistry, University of Southern California, Los Angeles, CA 90089-0482, USA*

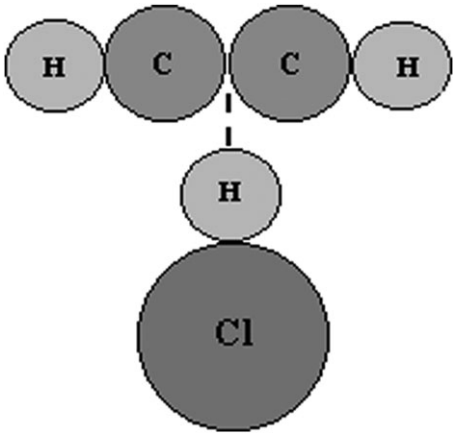

Fig. 1 Equilibrium structure of the C_2H_2–HCl H-bonded complex

geometry is well established.[6,7] The equilibrium geometry of the HCl/DCl complex is displayed in Fig. 1. More recently, emphasis has been placed on the dynamical properties of these species, particularly their VP behaviour, following excitation into modes localised primarily in either the C_2H_2 or the diatomic component of the H-bonded pair.[5,8–10] The results of these experiments indicate (1) that the dissociation pathways are strongly dependent on the manner of initial excitation and (2) the distributions among fragment states are rarely statistical. The results reported here on pair-correlated distributions are among the most highly resolved data available to date. They consist of correlated rovibrational distributions of fragment states following excitation of the asym C–H stretch in C_2H_2–DCl and similarly correlated distributions reported by Li *et al.*[5] in which VP was initiated by excitation into either HCl or C_2H_2 vibrational modes of the C_2H_2–HCl complex. Detailed analysis of these experiments reveals new insights into the mechanism by which energy-rich, H-bonded species fragment.

2. Experimental data and method of analysis

The experiment has been described in detail by Li *et al.*[5] and is summarised briefly here. Methods differ only slightly for the two H-bonded species considered. For the HCl complex, two different modes of excitation were employed. In the first of these the dimer is excited in $v = 1$ of the asym C–H stretch and, in the second one, in $v = 1$ of the HCl stretch. For the C_2H_2–DCl dimer, only $v = 1$ of the asym C–H stretch was excited. In each instance the *pair-correlated* distributions are determined, thereby linking the C_2H_2 fragment rovibrational distribution to individual rotational levels of $v = 0$ HCl/DCl. The rotational populations of the $v = 0$ H(D)Cl fragment were analysed using REMPI spectroscopy. Only a sub-set of $j_{H(D)Cl}$ states was found to be populated in each experiment, namely j_{HCl} = 4–7 and 6–8 for asym-C–H stretch and HCl stretch excitation respectively and j_{DCl} = 6–9. No population was detected in the $v = 1$ level of H(D)Cl. The centre-of-mass (c.m.) translational energies of the C_2H_2 fragments, in coincidence with each individual HCl/DCl rotational state, were obtained using velocity map imaging (VMI).[5] This yields a set of images of the velocity distribution for each individual

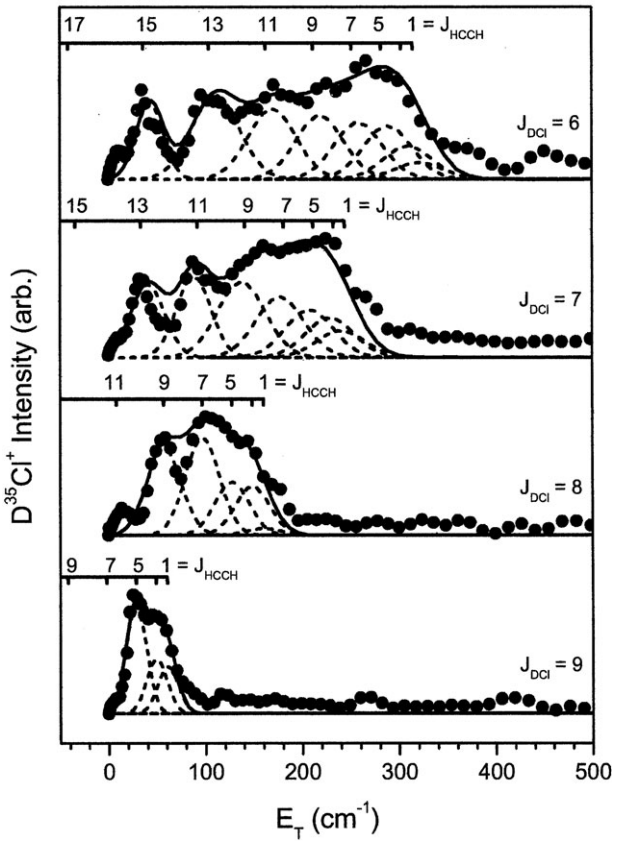

Fig. 2 Translational energy distributions of acetylene correlated with specific rotational levels of DCl, following excitation of the asym C–H stretch fundamental. The corresponding rotational levels of the acetylene co-fragment are indicated. Gaussian fits to individual $j_{C_2H_2}$ intensities, from which rotational populations are extracted, are shown dashed.

$j_{H(D)Cl}$ state with a resolution of around 30 m s^{-1}. This is sufficient to resolve the acetylene rotational distributions associated with each $j_{H(D)Cl}$ with C_2H_2 states identified using energy and momentum conservation. Thus the correlated rotational distributions within a single, uniquely identifiable C_2H_2 vibrational level were obtained following acetylene excitation and for a limited range of acetylene vibrational states in the case of HCl excitation. Results of this process for $j_{C_2H_2}$ within the ν_2 C–C stretch, correlated with j_{DCl} = 6–9, are shown in Fig. 2. Note that the parity of the K_a state selected in the excitation step determines whether odd or even rotational states of the C_2H_2 fragment are populated.[5] For both dimers excitation was *via* K_a 2 ← 1 and thus odd $j_{C_2H_2}$ were only observed for both C_2H_2–HCl and C_2H_2–DCl in the case of asym C–H stretch excitation. When HCl stretch excitation initiated VP, individual K_a levels were not resolved on excitation and so both odd and even fragment $j_{C_2H_2}$ are observed.

Fragment rotational state distributions for both H-bonded species are discussed in greater detail below but here we draw attention to a remarkable selectivity in fragment vibrational states that are populated on dissociation, one that depends strongly on the manner of excitation. In both C_2H_2–HCl and C_2H_2–DCl, VP initiated *via* the asym C–H stretch in the dimer populates rotational levels of the symmetric C–C stretch (ν_2)

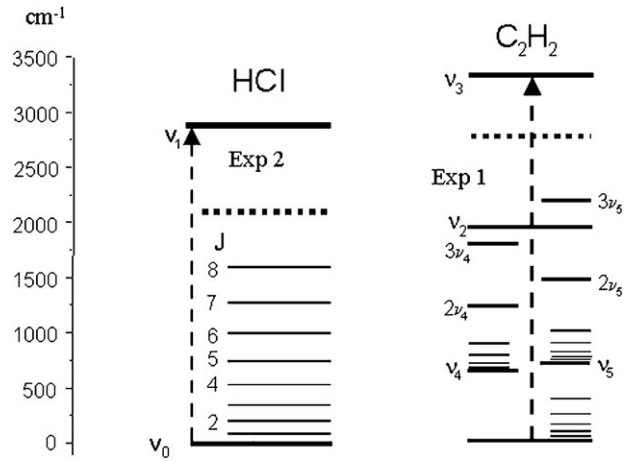

Fig. 3 Energy level diagram for the separate fragments of the C_2H_2–HCl H-bonded dimer showing the two modes of vibrational excitation (vertical broken arrows), excess energy available (horizontal dotted lines) and the rovibrational states accessible as energy acceptors.

and H(D)Cl $v = 0$ exclusively. Following HCl stretch excitation in C_2H_2–HCl, only acetylene bend modes (ν_4 and ν_5) are populated. A similarly high degree of selectivity was noted by Oudejans *et al.*[9,10] in the VP of the analogous C_2H_2–HF complex when excited *via* asym C–H stretch and the HF stretch. The energy level diagram of Fig. 3 indicates destination states accessible to each fragment in the C_2H_2–HCl dissociation. The dissociation energy of the HCl complex[5,11] is 700 ± 10 cm^{-1}. That of C_2H_2–DCl was determined here to be 755 ± 10 cm^{-1}. The excess energy available following HCl stretch excitation at 2806.9 cm^{-1} in C_2H_2–HCl is 2107 cm^{-1}, whereas following asym C–H stretch excitation ($\sim$3280 cm^{-1}), it is 2581 and 2527 cm^{-1} for the HCl and DCl complexes, respectively.

2.1 Theoretical analysis; the AM model

Two significant features of VP data in the acetylene–H(D)Cl dimers require theoretical justification, the first being the high degree of specificity among fragment vibrational states mentioned above and the second the rotational distributions within vibrational states accessed. The latter is conventionally expressed in terms of the partitioning of energy between rotation and translation. More precisely this division is between fragment rotational AM and recoil orbital AM (l_{rec}). Questions that spring to mind include: in what manner these observations are related; what they reveal concerning the VP process; and whether they are representative of more widespread features of VP in complex systems. Full quantum-mechanical treatment is not feasible and in the absence of a potential energy surface (PES), classical mechanics is not an obvious option. Furthermore these methods have not generally given insight into the relationship between cause and effect in the VP process, with few transferable principles emerging from studies undertaken. As with many of the molecular events falling within the general category of energy transfer, VP primarily consists of changes in *nuclear momentum* in which *e.g.* momentum of collision, or of vibration, is converted into rotational and/or orbital AM. Hence a nuclear dynamical formulation could be seen as the natural representation for collision–induced change.

In the AM model, force results from momentum change among or between assemblies of nuclei [12] rather than *via* the PES, as in the classical mechanics of Lagrange or Hamilton. Simple expressions represent the conversion of relative motion into vibration and/or rotation, or into recoil, without recourse to a PES. Momentum exchange is expressed as a state-to-state event in which quantisation and energy conservation are imposed as constraints. A significant element in this process is the conversion of relative motion into molecular rotation. This may be viewed as linear-to-angular momentum conversion or as creation, initially, of orbital AM in the interaction, that is then disposed as rotation and recoil orbital AM. In either formulation, an effective impact parameter (b_n), or molecular lever arm, is required to convert a linear- to angular momentum. Analysis of experimental data has shown[13] that this lever- or torque-arm is invariably of molecular dimension, having maximum value (b_n^{max}) = half bond length (HBL) in a homonuclear diatomic and an equivalent distance from the centre-of-mass (c.m.) in heteronuclear species.

Quantitative calculations of rotational distributions are based on the physical principles of the AM model and use a 3D ellipsoid representation of the molecule of interest to generate an appropriate molecular lever arm distribution.[12] In the VP of vdW complexes, high rotational excitation within the fragments is often observed and is attributed to interaction with the repulsive part of the potential energy surface. Bosanac[14] has demonstrated that torque, generated *via* $dV(R, \theta)/d\theta$, of magnitude sufficient to induce rotational state change, is available *only* at the repulsive wall of a PES, the angular variation of potential $V(R, \theta)$ in the attractive region being too slow for this purpose. This is one of the reasons that impulsive models are effective in describing energy exchange processes and hard shape representations have been widely used to describe the physics of collisions.[15] The first usage of the 3D ellipsoid in collision dynamical studies was by Kreutz and Flynn.[16] The value of this shape lies in its ability to give an accurate representation of $P(b_n\cos\varphi)$, the probability density of effective impact parameter, as a function of b_n. Quantitative agreement is obtained with experiment using ellipsoid dimensions $(a-b)$ = HBL where a and b are semi-major and semi-minor axes, respectively. Extension of this model to mass-asymmetric species is straightforward.[17] The method was developed initially for collision-induced vibration–rotation transfer (VRT) and collisions are simulated by a Monte Carlo—generated set of random trajectories that sample all regions of the ellipsoid surface and hence all values of b_n up to b_n^{max}. The general expression for j-change in VRT is;

$$\Delta j = \sqrt{\frac{\frac{1}{2}\mu v_r^2 - \Delta v\hbar\omega}{B} + \left(j_i + \frac{1}{2}\right)^2} - \left(j_i + \frac{1}{2}\right) \qquad (1)$$

where $\Delta v = v_f - v_i$, $\Delta j = j_f - j_i$, B is the rotational constant and $\hbar\omega$ is the vibrational energy. eqn (1) corrects a previously published[12,17,18] erroneous form of this equation.

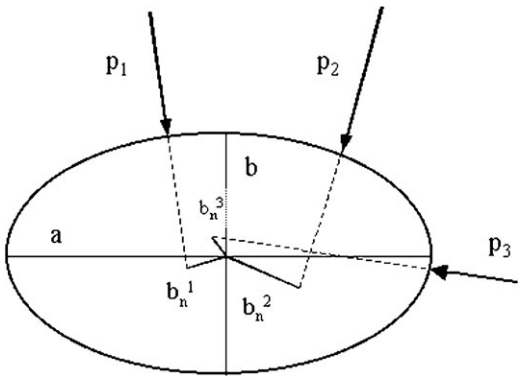

Fig. 4 Diagram to demonstrate that momentum (p) impacting on different points of the ellipsoid surface generates effective impact parameters (b_n) of different magnitude. Impulse normal to major or minor axes generates $b_n = 0$ only.

Vibrational predissociation of weakly-bound complexes is envisaged as a form of VRT in which 'internal collisions', the result of highly directional jostling by atoms of vibrationally excited species, induce transitions within and/or between vibrational modes and, simultaneously, generate rotational and orbital angular momentum. In a weakly bound complex there are bend and stretch modes involving the weak intermolecular bond, the latter facilitating the internal collision while the former allowing the system to explore potential dissociation geometries. This forms the conceptual basis of a model of VP introduced recently by McCaffery and Marsh.[18] Note that a significant difference between VRT and VP is that in the latter, the range of relative orientations of the subunits may be restricted in comparison to the case of an inelastic collision. The point of impact between the dimer components will be limited by the amplitude of the intermolecular bend mode and, in the case of C_2H_2–H(D)X species, this motion is about the centre-of-mass of the acetylene molecule. Thus, depending on the equilibrium geometry and the amplitude of the dimer bend motion, the full b_n^{max} value may not be achieved. This is illustrated in Fig. 4 in which the relationship between the point of impact on the ellipsoid surface and the magnitude of b_n is shown for three possible collision geometries. The maximum value of b_n is generated by impact normal to the surface at around 45° to the c.m. for the case that the c.m. is at the ellipsoid centre.

Calculation of rotational distributions following VP *via* the AM model are similar to those employed to predict the outcome of VRT in vibrationally excited species, though now b_n^{max} becomes a variable parameter, the maximum value of which is determined by the dimensions of the molecule concerned. Thus b_n can range up to HBL or its equivalent for a heteronuclear species. In HCl, for example, this is the distance from the c.m. to the H atom, *i.e.* 1.24 Å. In both C_2H_2–HCl and C_2H_2–DCl we find that the b_n values recovered from fitting data are generally less than the theoretical maximum available, suggesting that the bend motion of the dimer species is somewhat restricted. By contrast the VP of the benzene–Ar vdW complex from the 6^1 level occurs from a geometry well away from the c.m. of benzene[19] indicating wide amplitude in the vdW bend. The VP of rare gas-diatomic vdW molecules is also characterised by maximum b_n values close to the geometric limit.[18] Here, as in the case of C_2H_2–NH_3,[20] there is evidence of dissociation from more than one dimer geometry.

VP involving polyatomic species having more than one inertial axis introduces additional complexity. Sampson *et al.*[19] utilised an 'equivalent rotor' method to calculate rotational distributions of benzene following VP of the benzene–Ar vdW complex. This method, introduced to calculate VRT probabilities in 6^1 benzene, was tested by comparing calculated and experimental VRT data on a range of polyatomic species and is described in greater detail in the original work.[21] In this approach, rotations *about a specified inertial axis* are simulated by an equivalent (ellipsoidal) rotor having the rotational constant of the molecule about that axis and dimensions determined from the molecular structure perpendicular to that axis. Acetylene is particularly straightforward to model, as it is a linear rotor in its ground electronic state with c.m. mid-way between the two carbon atoms. The ellipsoidal parameters used here for C_2H_2 are $a = 2.11$ Å, $b = 0.6$ Å so that $b_n^{max} = (a - b) = 1.51$ Å.

3. Calculated distributions

Calculations were performed on C_2H_2–HCl and C_2H_2–DCl in the manner described above. The asym C–H stretch vibration was excited using 3281.4 cm^{-1} radiation in the first experiment, while HCl stretch excitation at 2806.9 cm^{-1} initiated dissociation in the second. In C_2H_2–DCl, VP was induced by asym C–H stretch excitation at 3282.04 cm^{-1}. In each experiment, destination vibrational levels in the fragments could be identified and so the energy available for disposal as rotation and/or orbital AM is known for each dissociation pathway. The calculations aim to reproduce the measured rotational distributions in order to obtain data on the geometric configuration of the dimer components at the moment of dissociation, inferred from the magnitude of b_n^{max}. This quantity was varied in computations of rotational distributions to obtain best fits to experiment and the results represent un-weighted sums of two or more calculated distributions. Thus more than a single VP geometry contribute to the population of fragment rovibrational states. The high quality and detail of the experimental data present a unique opportunity to consider the mechanism of VP and energy disposal processes in complex molecules more widely and this is addressed in the Discussion section.

Before describing destination state populations in detail we first consider the possibility that system-specific energy or angular momentum constraints control the partitioning of available energy into rotation and translation, *i.e.* the competition between fragment rotational and recoil orbital AM. This is a significant issue of relevance to models of VP where Ewing's rules[22] are often used as a first approximation to predissociation outcomes. Velocity–angular momentum diagrams have been used[18] to show that partitioning between product rotation and recoil is determined by molecular properties such as moment of inertia and bond length. Fig. 5 shows a velocity–AM diagram for the acetylene fragment following VP of the C_2H_2–HCl dimer initiated by asym C–H stretch excitation. Several possible outcomes are portrayed in this

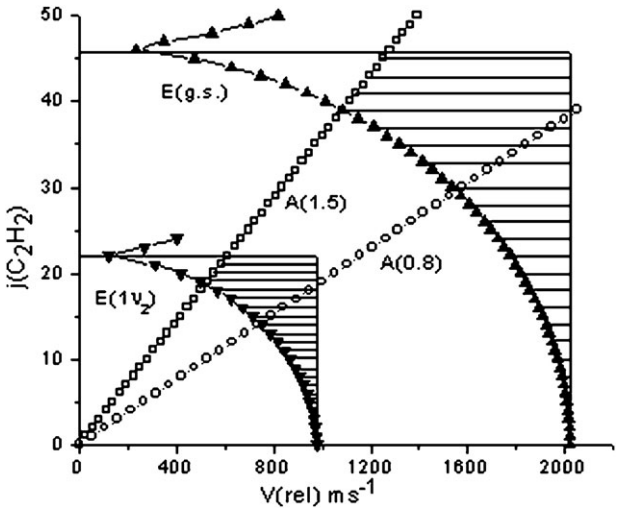

Fig. 5 Plot of fragment $j_{C_2H_2}$ *vs.* velocity for VP of C_2H_2–HCl following asym C–H stretch excitation. Plots are state-to-state threshold conditions for energy (E) and angular momentum (A) conservation expressed as relative velocity *vs.* C_2H_2 rotational state. Two VP routes are shown, one direct to rotational levels of ground state C_2H_2 (up triangles) and the other to rotational levels of the C–C symmetric stretch (ν_2) of the acetylene fragment (down triangles). A-Plots are drawn for $b_n^{max} = 1.51$ Å, the maximum theoretically available, and for 0.8 Å to represent a likely value accessed in the VP process. The shaded sections represent those regions of velocity–AM space for which conditions of energy and AM conservation are simultaneously met.

figure: (i) direct population of rotational levels of ground vibrational state of C_2H_2 and (ii) population of rotational levels of one quantum of the C–C stretch (ν_2) of C_2H_2 for the case (*a*) that all possible b_n values up to b_n^{max} are accessible and (*b*) for the situation where complex geometry and intermolecular bend vibration amplitude reduce the maximum b_n available to 0.8 Å.

Fig. 5 demonstrates that when the full theoretical maximum b_n value is utilised, energetic constraints do *not* restrict access to (energetically open) $j_{C_2H_2}$ states, a result of a large lever arm and high reduced mass in this system. The figure suggests that for fragment C_2H_2, $j \sim 40$ might be particularly favoured since this transition requires little energy change. However, the probability of generating rotational angular momentum falls rapidly as j increases and thus it is unlikely that the excited dimer will dissociate *via* this route. Large angular momentum 'loads' of this kind have been shown to constitute an exit channel barrier or bottleneck in exothermic processes such as VRT, VP and elementary reactions[23] and may ultimately prevent a process from occurring. The figure further demonstrates that when b_n^{max} is reduced, *e.g.* by restricted amplitude in the dimer bend mode, then the momentum conversion mechanism is much less effective and places an upper limit on j-values. Fig. 5 also demonstrates that the VP process would benefit if a proportion of available energy were deposited into a fragment *vibrational* state. On populating the C–C stretch the AM load is reduced very dramatically—by around 20 ħ for the case that $b_n^{max} = 1.5$ Å. Fragment vibrational modes represent energy repositories that are able to reduce

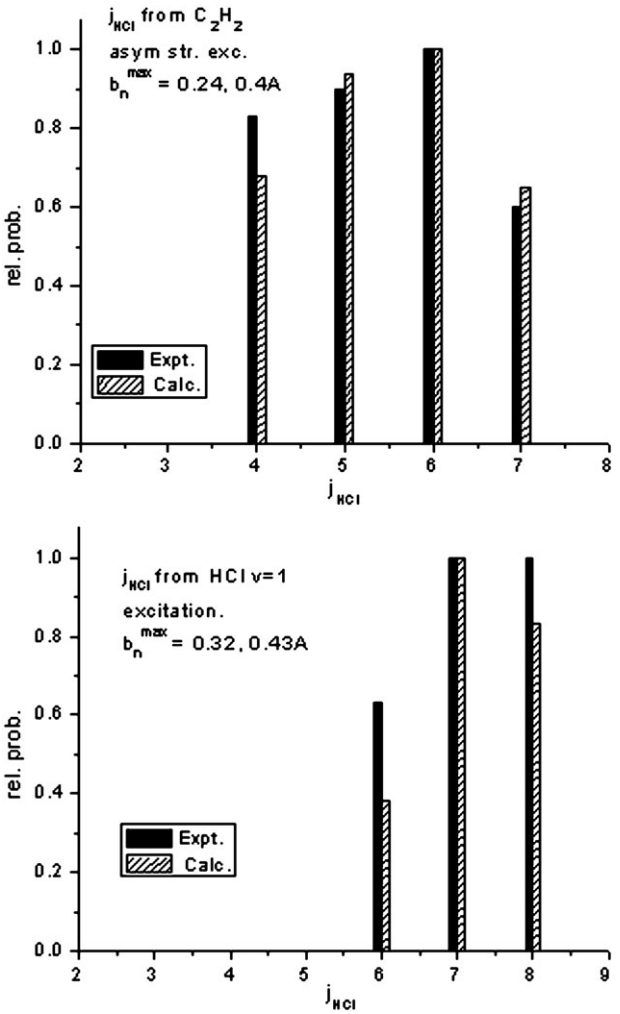

Fig. 6 Experimental and theoretical HCl rotational distribution following VP initiated by excitation of the asym C–H stretch (K_a $2 \leftarrow 1$) at 3281.4 cm^{-1} (upper panel). Values of b_n^{max} used to obtain fit were 0.24 and 0.40 Å. Experimental data from Table 2 of Li *et al.* are accurate to ±10%.[5] Lower panel, as above, but now excitation is *via* the HCl stretch Q band at 2806.9 cm^{-1}. b_n^{max} values = 0.32 and 0.43 Å.

both energy and AM load. Fig. 5 is drawn for the case that no HCl rotational states are populated and hence for VP to $1\nu_2$, around 600 cm^{-1} of energy must be disposed as C_2H_2 rotation and recoil orbital AM.

3.1 H(D)Cl rotational distributions

Fig. 6 shows experimental and calculated HCl ($v = 0$) fragment rotational populations following (i) excitation of the C_2H_2–HCl dimer *via* the $K_a = 2 \leftarrow 1$ transition in the asym C–H stretch at 3281.4 cm^{-1} and (ii) excitation *via* the Q branch of the HCl stretch at 2806.9 cm^{-1}. Note that the observation of rotational excitation in the H(D)Cl fragments indicates the diatomic cannot be in its equilibrium configuration at the moment of dissociation, *i.e.* the diatomic axis is tilted relative to the complex C_{2v} axis. Such a tilt would occur naturally as H(D)Cl oscillates about the equilibrium configuration in the dimer bend motion. Lower j_{HCl} states may also be populated

Table 1 Values of b_n^{max} used to fit experimental HCl fragment rotational distributions obtained by Li *et al.*[5] following asym C–H stretch and HCl stretch excitation of the dimer

HCl fragment.	
b_n^{max} values/Å	
C–H asym stretch exc.	HCl stretch exc.
0.24; 0.40	0.32; 0.43

but signal intensity above background is too small to be reliably estimated. The distribution is best regarded as one that is biased towards the mid- to high-j_{HCl} region.

Sufficient energy is released in the overall VP process in C_2H_2–HCl to populate up to $j_{HCl} = 15$ (asym C–H stretch excitation) and $j_{HCl} = 13$ (HCl excitation) but only a limited sub-set of middle range j_{HCl} values is observed. The patterns of the reliably measurable intensities however suggest that more than one configuration lead to dissociation. We note that throughout this work, rotational distributions measured by Li *et al.* are considered to be nascent. At even the lowest values of translational energy measured by Li *et al.*, separation velocity is several angstroms per picosecond and thus on dissociation the fragments move rapidly away from the region where impulsive forces are generated.

Fig. 6 shows calculated rotational state populations for the two cases considered. The states with measurable population are of very similar magnitude. As can be seen from the figures, theory is able to reproduce this unusual distribution but no single b_n^{max} was able to match the observed patterns. Rather, two values were needed to fit each set of data. These b_n^{max} values are listed in Table 1. In the case of asym C–H stretch excitation, the peaks at $j_{HCl} = 4$, 5 predominantly arise from impact at points giving $b_n^{max} = 0.24$ Å while the remaining two at $j = 6$, 7 are generated with $b_n^{max} = 0.4$ Å. As could be anticipated from the up-shifted j distribution, b_n^{max} values are somewhat larger when the HCl stretch initiates dissociation and are 0.32 and 0.43 Å. The maximum torque-arm available from the HCl diatomic is 1.06 Å and so the b_n^{max} values obtained from fitting experimental data indicate only a relatively small angle of tilt of the HCl bond at the moment of VP. The b_n^{max} values obtained by fitting data indicate that in both cases considered, VP occurs as a result of combined bend and stretch motions of the weak H-bond. The origin of these constrained distributions is discussed in section 4 below.

3.2 C_2H_2 rotational distributions

The rovibrational distributions in C_2H_2 are very sensitive to the excitation mode by which VP is induced and results from these two distinct modes are discussed separately.

(i) VP following asym C–H stretch excitation in C_2H_2–HCl and C_2H_2–DCl. The molecular motion of the asym C–H stretch in acetylene is shown in Fig. 7 together with that of other normal modes of this molecule. Following this form of excitation in the dimer, VP leads to population of the C–C sym stretch mode (ν_2) in acetylene exclusively. Thus all of the momentum and energy of the dissociation event are distributed between the rotational states of H(D)Cl ($v = 0$), of C_2H_2 (ν_2), and recoil. Li *et al.*[5] reported rotational distributions in

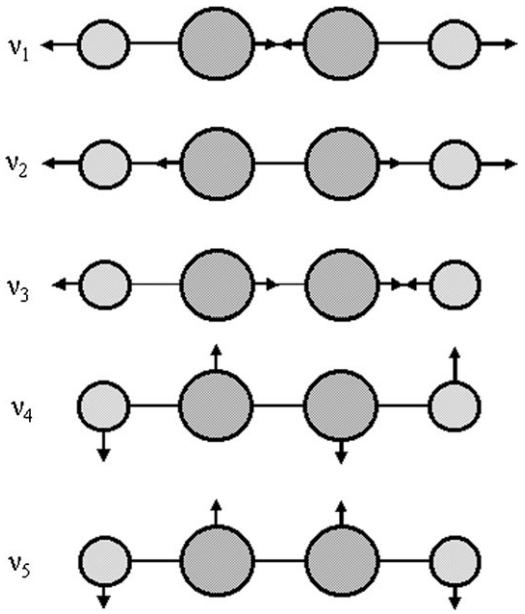

Fig. 7 The normal modes of acetylene.

C_2H_2 correlated with each individual rotational level of HCl and those from VP of C_2H_2–DCl are shown in Fig. 2. Thus for VP *via* the asym C–H stretch, eight separate C_2H_2 (ν_2) rotational distributions are available, one for each of $j_{HCl} = 4$–7 and $j_{DCl} = 6$–9. Different amounts of energy are available in each case and thus different distributions of rotational states ensue, indicating that several VP geometries are accessed.

The experimentally determined C_2H_2 (ν_2) distributions from VP of C_2H_2–HCl correlated with $j_{HCl} = 5$ and 6 are shown in Fig. 8. In each case there is substantial population in states up to the energetic limit. The distributions have high relative populations in mid-range $j_{C_2H_2}$ states but only small contribution at low j. In all cases other than $j_{HCl} = 7$, for which less than 22 cm^{-1} is available as C_2H_2 rotation, at least two values of b_n^{max} were needed to obtain a reasonable fit to data. Theory generally reproduces experimental data well, with the results shown in Fig. 8 being typical. The fit parameters (*i.e.* b_n^{max}) are listed in Table 2 and span a wide range of values. This suggests that there are few restrictions beyond the conservation laws on the generation of rotational angular momentum. The highest probabilities are found for geometries associated with mid to large values of b_n^{max}.

Rotational distributions following VP of C_2H_2–DCl follow a similar pattern, as seen in Fig. 9 where experimental and calculated C_2H_2 (ν_2) populations correlated with $j_{DCl} = 6$ are plotted. The calculation reproduces the data points within experimental error (±10%) but some six values of b_n^{max} were needed to obtain this level of agreement with the eight data points observed experimentally. Results of calculations on this system are given in Table 3 and these, together with data from calculations on C_2H_2–HCl listed in Table 2, suggest that each individual observable $[(v; j)_{H(D)Cl}; (v, j)_{C_2H_2}; l_{rec}]$ fragment state results from a near unique dissociation geometry for which $b_n \sim b_n^{max}$ and that geometries corresponding to excitation of all energetically allowed rotational levels are sampled.

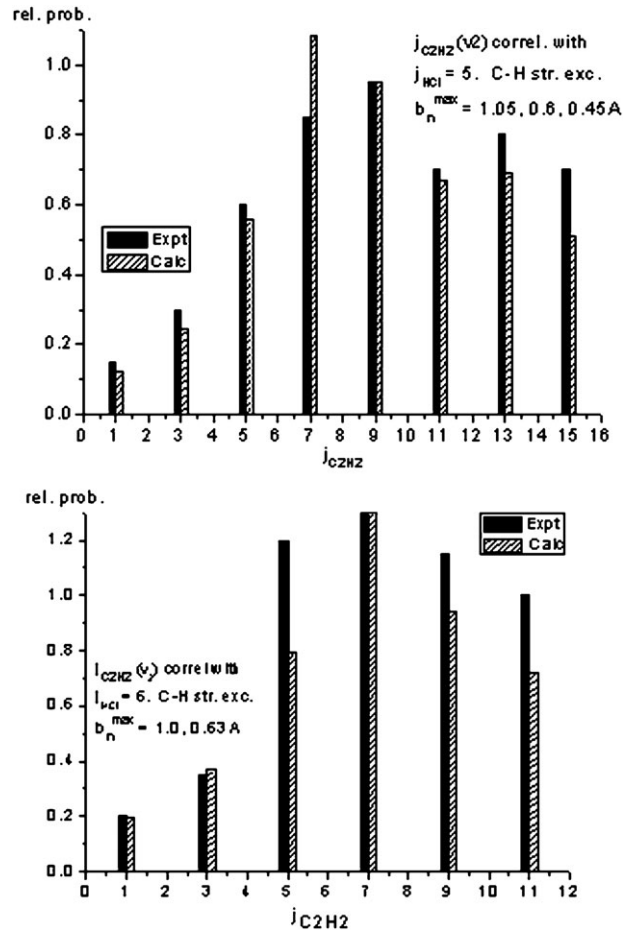

Fig. 8 Experimental and calculated $j_{C_2H_2}$ distribution in ν_2, the C–C stretch, correlated with $j_{HCl} = 5$ (upper panel) and $j_{HCl} = 6$ (lower panel). VP in this case follows excitation of the asym C–H stretch in the dimer. Experimental $j_{C_2H_2}$ values accurate to ±10%.

The acetylene *j*-distributions also quantify the partitioning between C_2H_2 and H(D)Cl rotation and recoil orbital AM of fragments. This topic is discussed in a later section but we note here that the process in which energy is deposited into a C_2H_2 acceptor vibration and one of the widely-spaced H(D)Cl rotational modes, greatly reduces the C_2H_2 AM load—a mechanism known to speed-up the VP process.[18] The partitioning of this reduced energy and AM load between C_2H_2 rotation and orbital AM varies quite widely. Furthermore the direction of l_{rec} relative to $j_{C_2H_2}$ and $j_{H(D)Cl}$ may be used by the system to meet overall AM conservation. Meeting these conservation relations while undergoing dissociation is a complex

Table 2 Values of b_n^{max} used to fit experimental C_2H_2 fragment rotational distributions correlated with individual j_{HCl} levels for the two forms of dimer activation

	C_2H_2 fragment. b_n^{max} values/Å	
j_{HCl}	C–H asym stretch exc.	HCl stretch exc.
4	0.3; 0.5; 0.7; 1.0	
5	0.45; 0.6; 1.05	
6	0.63; 1.0	0.36; 0.60; 0.9; 1.1
7	0.68	0.5; 0.66; 0.85; 1.05

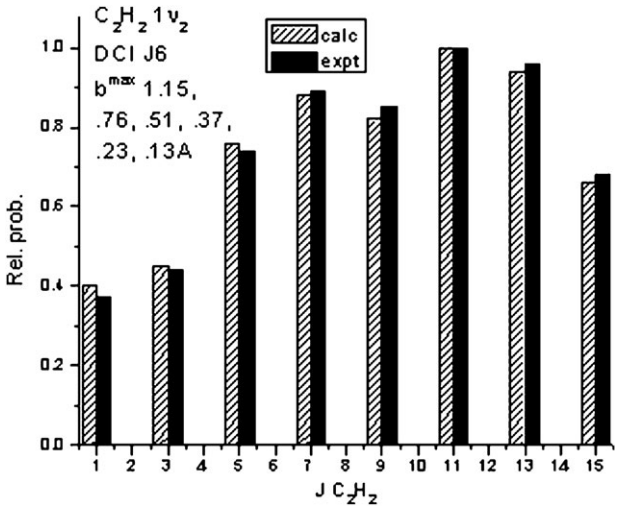

Fig. 9 Experimental and calculated $j_{C_2H_2}$ distribution in ν_2, the C–C stretch, correlated with $j_{DCl} = 6$. VP in this case follows excitation of the asym C–H stretch in the C_2H_2–DCl dimer.

task. However, the data suggest that numerous geometries and quantum pathways are available for VP, resulting in a reasonably efficient dissociation, as gauged by VP lifetime in the nanosecond range.

(ii) VP following HCl stretch excitation in C_2H_2–HCl. On exciting the HCl stretch vibration, the magnitude and direction of the dissociating impulse are changed and so fragment rovibrational distributions are expected that differ from those following asym C–H stretch excitation. The energy available, should the ν_2 C–C stretch mode be populated, would be sufficient to generate HCl in its lowest rovibrational states only, contrary to observation. Thus the C_2H_2 bends ν_4 and ν_5 become the principal acceptor modes in an AM load reduction strategy. As noted above, only $j_{HCl} = 6$, 7 and 8 levels are measurably populated and the c.m. translational energy distributions correlated with these appear rather similar in overall shape, peaking at modest recoil.[5] As with the populations described earlier, more than a single VP geometry appears to contribute to the overall VP process and angular momentum conservation does not constrain the C_2H_2 rotational distributions. The *j*-states of vibrationally excited C_2H_2 are again

Table 3 Experimental and calculated fragment C_2H_2 rotation state relative intensities in the (ν_2), C–C stretch vibration correlated with j_{DCl} = 6, 7, 8, 9 following asym C–H stretch excitation of the C_2H_2–DCl dimer. Experimental errors are ±10%

j_{DCl}	6		7		8		9	
$j_{C_2H_2}$	Expt	Calc	Expt	Calc	Expt	Calc	Expt	Calc
1	0.37	0.4	0.53	0.19	0.27	0.14	0.44	0.46
3	0.44	0.45	0.58	0.61	0.43	0.48	0.52	0.53
5	0.74	0.76	0.68	0.66	0.69	0.62	1	1
7	0.89	0.88	0.92	0.92	1	1		
9	0.85	0.82	1	1	0.87	0.87		
11	1	1	0.74	0.74				
13	0.96	0.94	0.65	0.64				
15	0.68	0.66						
b_n^{max}/Å	1.15; 0.76; 0.51; 0.37; 0.23; 0.13.		1.28; 0.75; 0.5; 0.36; 0.22.		0.85; 0.43.		0.8; 0.42; 0.18.	

populated up to the maximum allowed by energy conservation indicating that C_2H_2 rotation is generally favoured over fragment recoil. Several values of b_n^{max} are needed to fit the data and are similar in range and magnitude to those found when VP is initiated by C–H asym. stretch excitation.

Li *et al.*[5] were unable to obtain unique fits to these data sets because of the high density of rotational states in this spectral region. Nevertheless, they were able to show that the acetylene fragment is excited with one or two bending quanta. Rotational state intensities in this instance were taken from the band contours and therefore represent only approximations to the state-resolved probabilities. Adequate fits to these values were obtained assuming simultaneous excitation of two quanta of the ν_4 bend ($l = 0$) mode for $j_{HCl} = 6$, 7 though there are clear indications in the spectra that other states make some contribution. In particular, the combination $1_4 + 1\nu_5$, $2\nu_5$ and, for $j_{HCl} = 8$, $1\nu_5$ and $1\nu_4$ quite evidently contribute. The number of potential destination states increases rapidly in this region as states of non-zero vibrational angular momentum are accessed. Higher resolution would be needed to deconvolute these contributions. This high density of low $j_{C_2H_2}$ rotational states is very likely responsible for the close similarity of the distribution shapes found in this instance. Since there are no kinematic constraints, the observed distributions mainly reflect the influence of AM load on the maximum accessed $j_{C_2H_2}$.

3.3 Fragment vibrational state distributions

In each dimer considered here, and for each mode of initiating VP, one or more vibrational state of the C_2H_2 fragment is excited in the process of dissociation. Direct transfer to near-resonant *rotational* states of the ground vibrational state of each fragment does *not* occur in the species considered here despite the very small energy deficits involved. Thus following asym C–H stretch excitation, transition to $j_{C_2H_2} = 46$ disposes of all but 37 cm^{-1} of available energy while that to $j_{HCl} = 15$ leaves only 106 cm^{-1} to be found as C_2H_2 rotation and/or recoil. Similar near-resonant transitions are possible when HCl excitation initiates VP. These exit routes evidently are not favoured on dissociation, behaviour that follows a general propensity identified in exothermic inelastic, dissociative and reactive molecular events, namely that there is a limit to the angular momentum load a given energy-rich system may dispose of.[23] This barrier to exothermic molecular events has its origin in the exponential-like fall in probability of generating rotational AM as magnitude increases. At some point, for a given system, the transition probability for generating AM change becomes too small for the process to be detected. The deposition of substantial fractions of available energy into vibration reduces the AM load and greatly speeds vibration–rotation relaxation and VP.[18,23]

In molecules having many vibrational modes, relaxation processes are often remarkably selective[24] in a manner that is not well understood. Sampson *et al.*[19] suggested that transitions between vibrational states in inelastic and dissociative events require the initiating impulse to be in such a direction that the nuclear motion causing vibrational mode change additionally be capable of inducing the appropriate molecular rotation. These linked requirements constitute highly selective criteria on the nature of acceptor normal modes. The principle appears to apply to collision-induced vibrational relaxation in a number of polyatomics[21] and is consistent with the data of Li *et al.*[5] as well as that from C_2H_2–DCl reported here. The atomic motions characterising each of the normal modes of acetylene are shown in Fig. 7 from which the utility of this propensity rule may be gauged. When VP is initiated by C–H asym stretch excitation, the individual motions of nuclei are parallel to the molecular axis and are readily de-phased and slowed by collision with the proton of H(D)Cl as the hydrogen bond contracts. In this process the C–H stretch is relaxed to ν_2, the C–C sym. stretch, while released energy and momentum are transferred to C_2H_2 rotation, H(D)Cl rotation and fragment recoil on breaking the hydrogen bond.

When HCl stretch motion initiates the internal collision, impulse is primarily generated perpendicular to the C_2H_2 molecular axis, readily exciting bend modes, C_2H_2 rotations within ν_4 or ν_5, HCl rotation and recoil. Thus the simple principle outlined above appears to apply here. For $j_{HCl} = 8$, for example, acetylene fragments with one quantum of bend are excited because the AM load for acetylene is sufficiently low, whereas for lower j_{HCl} states, two quanta of bend are preferentially populated. Energy restrictions on HCl excitation prevent access to the acetylene ν_2 mode on VP and so this test of the general proposition is not wholly clear-cut. However, the influence of these geometric and kinematic factors is demonstrated in the VP of linear C_2H_2–NH_3.[20] Following excitation into the asym C–H stretch of acetylene, the predominant fragmentation channels are one quantum of the umbrella inversion mode of NH_3 coupled with bend modes of C_2H_2. Accessible vibrational modes that are not populated are NH_3 asymmetric bend (ν_4), ν_2 C–C stretch of acetylene and vibrational ground states of each fragment.

4. Discussion and conclusions

In the period since VP in weakly bonded vdW molecules was first observed[1] a number of theoretical approaches have been developed to explain and predict the widely varying lifetimes and fragment rovibrational distributions that characterise the dissociation of these species. These are briefly discussed here as the underlying physical principles of a theoretical method determine the information that approach may yield and several of the models proposed share a common theme. This short survey allows the findings reported here to be set in context. Theoretical methods employed over recent years have ranged from full solution of the close-coupled equations of scattering theory to selection and propensity rules based on relatively simple physical precepts. Despite this, no single approach has proved entirely satisfactory. Ideally a theory should reproduce experimental measurements in a reasonably quantitative fashion yet retain sufficient transparency that 'rule-of-thumb' guidance linking outcomes to known molecular properties may be identified. The detail and completeness of the information contained in modern experiments offer a unique opportunity to advance our theoretical insight.

Quite early in the development of the field, Hutson, Ashton and Leroy[25] performed close-coupled scattering calculations

on VP in H_2–Ar and isotopic variants. VP lifetimes were calculated from the energy dependence of the S-matrix eigenphase sum for individual quantum states, obtaining lifetimes $>20 \times 10^{-6}$ s. Little physical insight emerges *via* this approach and the authors were forced to resort to perturbation expressions for this purpose. Their conclusion, that the mechanism was dominated by higher order potential coupling terms, is not surprising given the high degree of fragment rotation that frequently accompanies VP. Hutson, Clary and Beswick[26] used the azimuthal and vibrational close coupling, rotational infinite order sudden method of Clary,[27] extending calculations of VP resonance widths to rare-gas—symmetric top complexes. A number of general principles linking outcomes to features of the PES have evolved[28] and relate to situations in which motion on a surface provides the motive force for dissociation. Fragment rotation is related to the form of the vdW bending wavefunction and/or interactions in exit channels as the fragments depart. In the impulsive limit, the free rotor expansion coefficients of the bending function determine the rotational distribution.

Few transferable rules-of-thumb emerged from these studies though, as is well documented, the perturbation theory approach and formulation of golden rule expressions for VP by Beswick and Jortner[29] and by Ewing[22] have been very fruitful in the development of a conceptually transparent model of VP and expressions that allow estimation of dissociative lifetime. The origins of these energy and momentum gap expression have been reviewed on numerous occasions.[2,30] In these formulations, the dependence of VP probability on the overlap between bound and continuum nuclear wavefunctions dictates that fragment translational motion will be constrained by this overlap factor. Thus very often, a substantial fraction of the energy released must take the form of fragment rotation. This two-dimensional picture of the VP process treats rotational energy as a balancing element in the overall energy conservation equation rather than an essential component of the mechanism.

With greater experimental emphasis on rotational distributions following VP, this simple approach through gap laws is found to be a useful guide for certain classes of van der Waals molecule, *e.g.* complexes of diatomic hydrides such as OH, HF *etc*. However, the method is less helpful in rationalising the energy partitioning in other systems, *e.g.* complexes of diatomic halogens. This dependence on molecule type was recently shown[18] to be the result of angular momentum constraints. These limit the range of rotational states accessible, often to well below the energetic limit. AM constraints in VP particularly affect molecules that have large moment of inertia and long bond length and this highlights a deficiency in the two-dimensional view of VP in which fragment rotation has no more than a residual role. Molecular dissociation is characterised by relative motion of the departing fragments and this is most generally written in terms of fragment orbital angular momentum (l_{rec}). All processes of molecular change are required to conserve angular momentum and that generated by the dissociating impulse must be balanced by the (vector sum of) rotational and orbital AM of the fragments.

Rotational distributions enter the 'golden rule' quantum formulation of VP explicitly when an angular dependence is added to radial variables of chemical and vdW bond distance, as introduced by Halberstadt, Beswick and Janda.[31] In this treatment, continuum–continuum couplings must be included in determining the continuum functions that provide comparison with experiment. These latter functions are expanded as products of vibrational functions and spherical harmonics. Calculations reproduce experimental rotational distributions and lifetimes, though are highly sensitive to details of the PES. In the case of $HeCl_2$, five parameters of the potential required adjustment to reproduce the unusual double-peaked *j*-distribution found experimentally. Relatively little insight into the origin of this or other distribution shapes emerges however and the method is limited to small molecules. The wave-packet dynamical calculation by Gray and Wozny[32] also reproduces the two-peak structure seen in the $HeCl_2$ rotational distribution. The structure is attributed to a quantum interference effect. However, it is not clear from the treatment why this vdW species is special in this respect.

Ewing[33] recognised the close similarity between vibration–rotation transfer and VP explicitly in deriving a selection rule for both processes that could be incorporated into a simple lifetime expression. This is based on the evident reluctance of an excited molecule to change quantum numbers in a relaxation process, concisely expressed in the principle that relaxation is only efficient when the total change in effective quantum numbers for the process is small. The formal expression of this principle[33] has an attractive simplicity being composed of a collision frequency factor and an exponential term in Δn_T, the total change in quantum numbers (vibration, rotation and translation). The computation of these changes is less simple, although the familiar bound–continuum wavefunction overlap plays a central part. The close link between VP and VRT is emphasised by Forrey *et al.*[34] These authors note that so-called quasi-resonant VRT, in which near-resonant, collision–induced, low Δj transitions involving $\Delta v = \pm 1$, fulfil the Ewing (Δn_T = small integer) criterion and are furthermore characterised by very narrow rotational distributions. Forrey *et al.* note that a selection rule not unlike that proposed by Ewing operates in the case of quasi-resonant VRT and constitutes a criterion based on conserved classical action. However, quasi-resonant VRT is restricted to a limited sub-set of diatomic molecules[35] while the formation and subsequent VP of vdW complexes is generally non-discriminating in respect of molecule type.

Conceptually distinct from the models surveyed above is that proposed by Kelley and Bernstein.[4] In their approach, VP is envisaged as a sequential process with intramolecular vibrational redistribution (IVR) occurring prior to dissociation. Once sufficient energy has migrated to the vdW modes, dissociation may be treated using a restricted form of RRKM theory in which only the vdW modes are considered. The model predicts VP lifetimes for aromatic molecule—rare gas complexes in reasonable agreement with experiment, though is not suitable for calculating rotational distributions. The authors point out the stringent conditions of energy match for IVR to occur and that this requires energy-resonant alternative configurations among the rovibrational energy levels of the molecule concerned. At the extreme of vdW dimer simplicity, IVR would not be expected to be significant but

becomes more probable as molecular complexity increases. The acetylene–HCl dimer is of intermediate density of states. The energy level density in the excitation region is such that IVR might be feasible if highly excited vdW modes are involved. The evidence for and against this is discussed in more detail below.

The AM model[18] of VP assumes an impulsive interaction that transfers momentum over a period that is short on a vibrational timescale. An off-centre impulse generates orbital AM (l_i) that, together with any initial dimer rotational AM (j_i), forms J_i the initial total AM. The probability that this initial impulse will be converted into fragment rotation is calculated for each state-resolved transition within the constraint that each must obey energy conservation. Thus the primary event is the conversion of impulse, initially generated by vibrational motion, into rotation with recoil now the residual or balancing item. This approach has successfully reproduced a wide range of experimental VP data on di- and polyatomic vdW species.[18–20] The method cannot, as presently formulated, be used to calculate VP lifetimes although a simple formula relating lifetime to the magnitude of AM load and molecular efficiency factors gives a rough guide.[18] The AM method uses quantities that are familiar in other chemical contexts such as bond length, mass, spectroscopic constants, and thus rule-of-thumb generalisations may be derived. The method has much to offer in the analysis of VP in a system as complex as C_2H_2–H(D)Cl and has successfully modelled VP in the analogous C_2H_2–NH_3 complex.[20] However, it does introduce an element not present in earlier theoretical methods discussed above, namely *momentum exchange* as the motive force for the dissociation with energy simply constituting a conservation constraint on the principal mechanism. Both operate on a state-to-state basis.

In a direct dissociation, J_i is converted into fragment species rotation plus recoil orbital AM, *i.e.* $j_{C_2H_2} + j_{HCl} + l_{rec}$ in the acetylene–HCl case. Total J must be conserved so that the vector sum of these component rotational angular momenta, together with recoil, must equal J_i. The magnitude of initial orbital AM will depend on the impact point of the internal collision and hence a number of different J_i values may be generated throughout the many cycles of intramolecular bend and stretch that occur prior to dissociation. Thus the molecule must seek pathways for dissociation that satisfy the AM conservation relation and, for each route chosen, also conserve energy. The experimental data suggest the operation of a form of hierarchy in energy disposal, with the largest quanta taking precedence over the smallest; *i.e.* C_2H_2 vibrational energy before HCl rotation, followed by C_2H_2 rotation, with l_{rec} available to meet conservation needs through fragment relative speed and direction. Thus dissociation requires the system to solve a complex algorithm in order for VP to occur. However the problems that arise from angular momentum disposal are diminished when large fractions of the excess energy can be deposited into vibrational modes of one or more of the fragments.

Indirect evidence of the influence of the above-mentioned factors is available in the VP of van der Waals dimers containing diatomic[18] and polyatomic[19,20] molecules. The work reported here and that of Li *et al.*[5] is noteworthy in that a complete determination of the states populated in *both* fragments was achieved with quantum states in the C_2H_2 fragment correlated with those in H(D)Cl. We have shown here that rovibrational distributions among the fragments obtained experimentally may be reproduced using a simple, transparent model of VP. Are there new causative relationships that may be deduced from these data? In what follows we summarise the findings of this study and end by stating the principal conclusions.

First we consider the hierarchical element, mentioned above, in which processes depositing the largest energy quanta set conditions on those lower down the scale of quantum size. Population of HCl $v = 1$ is not feasible on energy grounds for either form of initial excitation. In experiments on C_2H_2–DCl, vibrationally excited DCl fragments have not been observed following C–H excitation. Direct vibration–rotation conversion to high-lying j-states of C_2H_2 $v = 0$ is highly unlikely on the grounds that the AM magnitude is too large to have significant probability. Similar arguments apply to near-resonant j-states of H(D)Cl $v = 0$. Potential energy acceptor states therefore are those accessible vibrational modes of C_2H_2 namely the fundamental in ν_2 (C–C stretch), and fundamentals, overtones and combinations of ν_4 and ν_5, the bend modes.

In the first step of VP, the energy-rich molecule reduces the AM load by dumping a substantial fraction of its available energy into a suitable fragment high-energy (usually vibrational) mode. This step appears to be important in ensuring an efficient dissociation pathway. VP following asym C–H stretch excitation leads to population of the ν_2 C–C stretch while that following HCl excitation yields C_2H_2 fragments in bend modes, outcomes that are predictable from the motions of the normal modes in conjunction with the principle[19] that the impulse causing state change be in such a direction that rotation may be simultaneously excited in the final vibrational state. The results of experiments discussed here and on C_2H_2–NH_3 [20] support this propensity rule. Note however that in the related C_2H_2–HF dimer, there is evidence[8] that VP initiated by HF excitation preferentially deposits the major fraction of available energy into HF rotation in a dissociation that is faster than those discussed here. The experimental method does not involve direct determination of quantum state populations, which are inferred from fragment angular distribution measurements.[8] C_2H_2–HF may represent a special case in which the energy and AM algorithm the weakly-bound species must solve in order to dissociate is particularly simple. In this instance $j_{HF} = 11$, the dominant channel, leaves sufficient energy remaining to access $j_{C_2H_2} = 3$ in the acetylene ground vibrational state. Values of b_n^{max} required to achieve these in the fragments are quite modest, as is that to produce an appropriate J_i. Also, the large rotational constant of HF allows the disposal of significant amount of energy into relative few rotational quanta.

Once the complex has identified a suitable energy dump mode for the major fraction of available energy, attention focuses on processes involving the next largest quanta, here in the H(D)Cl rotational modes. As noted above, the H(D)Cl rotational distributions for both modes of excitation have maximum values in $j_{HCl} = 4$–7 and $j_{DCl} = 6$–9 following asym C–H stretch excitation and $j_{HCl} = 6$–8 when HCl stretch is

excited. The upper limit on $j_{H(D)Cl}$ in each instance is set by energy limitations once the major portion has been disposed into the C–C stretch in the former case and into overtone and combinations of the bend modes in the latter. Routes involving bend mode *fundamentals* with consequent high $j_{C_2H_2}$ are little populated and, more generally, experiment suggests that pathways involving $j_{C_2H_2} > 20$ are disfavoured. All observed rotational states are associated with impact parameters that are well within the range of motion of intermolecular vibrational modes of the complex.

The final disposal into the smallest quanta, *i.e.* the rotational states of C_2H_2 and accompanying recoil orbital AM is determined by the need to conserve overall energy and AM while minimizing the AM load. In each excitation regime, C_2H_2 rotational levels up to the energetic maximum are observed for each j_{HCl}. In the case of HCl stretch excitation, the potential final state level density among the bend overtones and combinations is too great for a clear identification to be made, though the data demonstrate that bending levels in C_2H_2 are always excited. Indeed, a reasonable fit to band contours for $j_{HCl} = 6$, 7 was obtained assuming $2\nu_4$ to be the destination state. Though conclusions regarding detailed partitioning between orbital and rotational AM are difficult to make, the data indicate that for each j_{HCl} the most efficient VP routes are those for which the AM load is manageable. From the well-resolved C_2H_2 rotational distributions following asym C–H stretch excitation, it is clear that disposal of the small remnants of energy and AM is rather democratic among rotation and orbital AM. This fits well with findings from the theoretical analysis that several relative geometries of the molecular subunits are active in the dissociation.

In the preceding discussion of momentum exchange, a direct, impulsive model of VP in which the excitation energy remains localised until the instant of dissociation was used. This is a sensible approach, considering the difficulties in exact calculations for weakly bound dimers. Other approximate models have been used to describe VP, and these are complementary to the approach described here. For example, a common interpretation involves energy flow through resonant vibrational modes into the reaction coordinate in order for dissociation to occur. Even in the absence of exact energy-resonant configurations in each subunit, the zeroth order states can evolve *via* eigenstates of the complex that include coupling to intermolecular bend and stretch intermolecular modes in high quantum states. These intermolecular modes together with the C–C stretch and bend form the bath states into which the initial excitation flows in a concerted step, as the excited dimer evolves into dissociated fragments. Four low-frequency intermolecular bend and stretch modes exist that are strongly coupled through anharmonic terms and these can evolve into the fragment rotor states and recoil orbital AM that are seen experimentally.

Several summarising comments of wider relevance to VP in general and to low-energy breaking of H-bonds in other contexts can be made on the basis of the analysis of the results of Li *et al.*[5] on VP in C_2H_2–HCl and those reported here on C_2H_2–DCl. These are listed below.

1. In processes involving 'large' molecules, VP is more complex than can be dealt with by application of Ewing's rules alone. The dissociation no longer hinges on a simple competition between rotation and recoil orbital AM. Now vibration–rotation, rotation–rotation as well as rotation–recoil competition determines the outcome of the VP event.

2. The role of nuclear motion is central to the dissociation of these chemically and biologically significant systems. A static model involving no more than electron displacement could not account for the experimental observations.

3. Whether or not IVR necessarily precedes VP depends on the specific system under consideration. The treatment here does not assume IVR as a prerequisite but a perfectly valid, if cumbersome, theory including partial IVR could probably account for the observations.

4. Several configurations of the dimer components may lead to dissociation, each of which appears to be of roughly equal probability. Each entails deposition of a large fraction of available energy into a C_2H_2 vibrational mode and smaller amounts of energy into available HCl or DCl rotations. The upper limit to $j_{H(D)Cl}$ is set once the initial step is determined. Lower limits on $j_{H(D)Cl}$ are less clear-cut and may be a consequence of the AM load created for $j_{C_2H_2}$ if too much energy remains. Pathways with $j_{C_2H_2} > 20$ appear generally to be disfavoured. Remaining, unused energy is disposed into C_2H_2 rotation and recoil orbital AM. Sharing between these appears to be quite flexible within the constraints of meeting overall energy and AM conservation and limits set by the higher level processes.

5. Calculations based on the internal collision AM model reproduce experimental data and yield information on geometry at the moment of dissociation. Taken together with more general principles deduced from related work, some rule-of-thumb predictability regarding the outcome of VP in complex molecules may be feasible.

6. Vibrational predissociation in C_2H_2–H(D)Cl, a complex problem when formulated in quantum or classical mechanical terms, is relatively straightforward to describe using the method outlined here. In this, VP may be related to conventional chemical representations of molecules and their known vibrational motions, as well as the mechanism by which they proceed to the dissociation coordinate.

Acknowledgements

HR is grateful to the US National Science Foundation for supporting this work. We thank Blithe Casterline and Igor Fedorov for help in the experimental part of this work.

References

1 (*a*) R. E. Smalley, D. H. Levy and L. Wharton, *J. Chem. Phys.*, 1976, **64**, 3266–3276; (*b*) M. S. Kim, R. E. Smalley, L. Wharton and D. H. Levy, *J. Chem. Phys.*, 1976, **65**, 1216–1217.
2 M. I. Lester, *Adv. Chem. Phys.*, 1996, **96**, 51–102.
3 T. Baer and W. L. Hase, *Unimolecular Reaction Dynamics: Theory and Experiment*, OUP, Oxford, 1996.
4 D. F. Kelley and E. R. Bernstein, *J. Phys. Chem.*, 1986, **90**, 5164.
5 G. Li, J. Parr, I. Federov and H. Reisler, *Phys. Chem. Chem. Phys.*, 2006, **8**, 2915–2924.
6 A. C. Legon, P. D. Aldrich and W. H. Flygare, *J. Chem. Phys.*, 1981, **75**, 625–630.
7 J. B. Davey, M. E. Greenslade, M. D. Marshall, M. D. Wheeler and M. I. Lester, *J. Chem. Phys.*, 2004, **121**, 3009–3029.

8 D. C. Dayton, P. A. Block and R. E. Miller, *J. Phys. Chem.*, 1991, **95**, 2881–2888.
9 L. Oudejans and R. E. Miller, *J. Phys. Chem. A*, 1999, **103**, 4791–4797.
10 (*a*) L. Oudejans, D. T. Moore and R. E. Miller, *J. Chem. Phys.*, 1999, **110**, 209–213; (*b*) Erratum,, *J. Chem. Phys.*, 1999, **110**, 7109.
11 P. Carcabal, V. Brenner, N. Halberstadt and P. Millie, *Chem. Phys. Lett.*, 2001, **336**, 335–342.
12 A. J. McCaffery, *Phys. Chem. Chem. Phys.*, 2004, **6**, 1637–1657.
13 M. Osborne and A. J. McCaffery, *J. Chem. Phys.*, 1994, **101**, 5604–5614.
14 S. Bosanac, *Phys. Rev. A: At., Mol., Opt. Phys.*, 1981, **26**, 816–824.
15 H. J. Korsch and E. Ernesti, *J. Phys. B* , 1992, **25**, 3565–3599.
16 T. G. Kreutz and G. W. Flynn, *J. Chem. Phys.*, 1990, **93**, 452–465.
17 R. J. Marsh and A. J. McCaffery, *J. Phys. B: At. Opt. Mol. Phys.*, 2003, **36**, 1363–1382.
18 A. J. McCaffery and R. J. Marsh, *J. Chem. Phys.*, 2002, **117**, 9275–9285.
19 R. K. Sampson, S. M. Bellm, A. J. McCaffery and W. D. Lawrance, *J. Chem. Phys.*, 2005, **122**, 074311.
20 J. A. Parr, G. Li, I. Federov, A. J. McCaffery and H. Reisler, *J. Phys. Chem. A*, 2007, **111**, 7589–7598.
21 A. J. McCaffery, M. A. Osborne, R. J. Marsh, W. D. Lawrance and E. R. Waclawik, *J. Chem. Phys.*, 2004, **121**, 169–180.
22 (*a*) G. Ewing, *J. Chem. Phys.*, 1979, **71**, 3143–3144; (*b*) G. Ewing, *J. Chem. Phys.*, 1980, **72**, 2096–2107.
23 A. J. McCaffery, M. A. Osborne and R. J. Marsh, *J. Phys. Chem. A*, 2005, **109**, 5005–5015.
24 G. W. Flynn, C. S. Parmenter and A. M. Wodtke, *J. Phys. Chem.*, 1996, **100**, 12817–12838.
25 J. M. Hutson, C. J. Ashton and R. J. LeRoy, *J. Phys. Chem.*, 1983, **87**, 2713–2720.
26 J. M. Hutson, D. C. Clary and J. A. Beswick, *J. Chem. Phys.*, 1984, **81**, 4474–4480.
27 D. C. Clary, *J. Chem. Phys.*, 1984, **81**, 4466–4473.
28 R. Schinke, *Photodissociation Dynamics*, CUP, Cambridge, 1993.
29 A. Beswick and J. Jortner, *J. Chem. Phys.*, 1978, **68**, 2277–2279.
30 A. Rohrbacher, N. Halberstadt and K. Janda, *Annu. Rev. Phys. Chem.*, 2000, **51**, 405–433.
31 N. Halberstadt, A. Beswick and K. C. Janda, *J. Chem. Phys.*, 1987, **87**, 3966–3975.
32 S. K. Gray and C. E. Wozny, *J. Chem. Phys.*, 1989, **91**, 7671–7684.
33 G. Ewing, *J. Phys. Chem.*, 1987, **91**, 4662–4671.
34 R. C. Forrey, N. Balakrishnan, A. Dalgarno, M. R. Haggerty and E. J. Heller, *Phys. Rev. A: At., Mol., Opt. Phys.*, 2001, **64**, 022706.
35 S. Clare and A. J. McCaffery, *J. Phys. B*, 2000, **33**, 1121–1134.

